# Drawing of Ultrahigh Molecular Weight Polyethylene Fibers in the Presence of Supercritical Carbon Dioxide

MANUEL GARCIA-LEINER,[1] JOHN SONG,[2] ALAN J. LESSER[1]

[1]Polymer Science & Engineering Department, University of Massachusetts–Amherst, Amherst, Massachusetts 01003

[2]U.S. Army Soldier Systems Command RD&E Center, Natick, Massachusetts 01760

*Received 8 May 2002; revised 25 February 2003; accepted 28 February 2003*

**ABSTRACT:** The drawing behavior of ultrahigh molecular weight polyethylene fibers in supercritical carbon dioxide ($scCO_2$) is compared to that in air at different temperatures. The temperature substantially influences the drawing properties in air, whereas in $scCO_2$, a constant draw stress and tensile strength are observed. Differential scanning calorimetry shows an apparent development of a hexagonal phase along with a significant increase in the crystallinity of air-drawn samples with increasing temperature. The existence of this phase is not confirmed by wide-angle X-ray scattering, which instead shows that air-drawn samples crystallize in an internally constrained manner. In contrast, $scCO_2$ allows crystals to grow without constraints through a possible crystal–crystal transformation, increasing the processing temperature to 110 °C. © 2003 Wiley Periodicals, Inc. J Polym Sci Part B: Polym Phys 41: 1375–1383, 2003
**Keywords:** drawing; ultrahigh molecular weight polyethylene fibers; supercritical carbon dioxide; mechanical properties; polymorphism

## INTRODUCTION

The commercial and practical relevance of polyethylene has grown significantly since it was introduced into everyday life. Currently, polyethylene materials are synthesized and processed to attain properties particularly suited for specific applications. In this sense, several strategies have been proposed to obtain high-modulus polyethylene fibers.[1] Ultrahigh molecular weight polyethylene (UHMWPE) fibers represent the first case of a successful conversion of a flexible polymer into an ultrastrong fiber, and they have rapidly gained acceptance in many applications in which high strength and modulus are required.[2] The processing conditions under which a polymeric fiber is drawn have been shown to play an important role in its final properties. Many investigations have suggested that the ultimate properties of UHMWPE materials are remarkably influenced by their specific drawing conditions, including the drawing temperature and rate.[3,4]

Supercritical carbon dioxide ($scCO_2$) has proven to be an environmentally friendly alternative for a wide range of applications. At supercritical conditions, $CO_2$ has a unique combination of properties from both liquid and gas states, exhibiting liquidlike densities combined with low viscosities and high diffusion rates characteristic of a gas phase.[5–12] Because of the high compressibility of $scCO_2$, its solvent properties can be tuned and controlled by small changes in temperature and pressure; it acts as a reversible plasticizer that can easily be removed from the system during depressurization, leaving the final product solvent-free and reducing the costs of solvent removal.[13] With some particular exceptions, $scCO_2$

Journal of Polymer Science: Part B: Polymer Physics, Vol. 41, 1375–1383 (2003)
© 2003 Wiley Periodicals, Inc.

is a nonsolvent for most polymers, but it can plasticize most very efficiently. Recently, several strategies have been used to design $scCO_2$-philic materials to overcome the poor solubility of most materials in $scCO_2$.[6,7,12]

In general, it is widely accepted that the interaction of $scCO_2$ with a semicrystalline polymer is selective to the amorphous phase and under certain conditions can induce crystallization.[14] Hobbs and Lesser[15,16] showed that the final properties of poly(ethylene terephthalate) fibers drawn by a two-stage process were considerably affected by the presence of $scCO_2$, reporting significant increases in the elastic modulus and strength for $scCO_2$-treated samples. Also, considerable effects have been observed in nylon-6,6 fibers: samples drawn in $scCO_2$ show significantly higher crystallinity and orientation along with improved mechanical properties.[17] Because this behavior is expected to be valid in other semicrystalline polymers as well, significant improvements in the ultimate properties of a polymer when drawn in the presence of $scCO_2$ are expected to occur.

In addition, the imposed hydrostatic pressure has been related to some experimentally observed changes as well. Crystal–crystal transitions have been detected for polyethylene when extreme conditions are imposed.[18–22] Under nonpermeable conditions, as for a highly crystalline material, the presence of $scCO_2$ may promote changes in the state of stress of drawing, imposing hydrostatic contributions to the principal stresses that in some cases must be able to modify the physical and mechanical properties of the deformed material. This effect has not been studied, and the overall hydrostatic contribution of $scCO_2$ in the drawing process has not been quantified and understood yet.

In this work, the *in situ* drawing behavior and the physical and mechanical properties of UHMWPE fibers drawn uniaxially in $scCO_2$ are compared to those observed when the deformation is performed in air. Significant differences are observed in the thermal and mechanical properties of $scCO_2$-drawn fibers with respect to air-drawn fibers at the same processing conditions. Because of the high crystallinity of these materials (>90%), a typical plasticization effect of $scCO_2$ in the amorphous phase is not expected. In contrast, the effect of the hydrostatic pressure brought about by the presence of $scCO_2$ is related to the observed changes in the properties of $scCO_2$-drawn fibers. Experimental data support the idea of a possible crystal–crystal transformation to the more mobile hexagonal phase because of a synergistic effect of the drawing temperature and the higher pressures imposed when the deformation is performed in $scCO_2$.

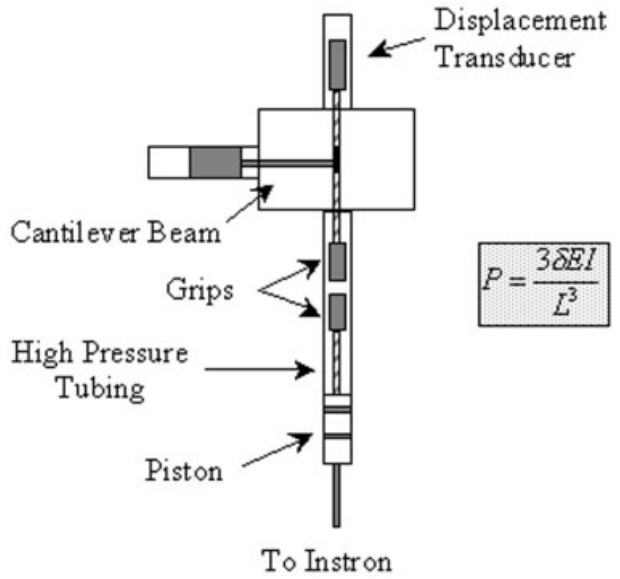


**Figure 1.** High-pressure drawing apparatus.

## EXPERIMENTAL

UHMWPE fibers (Spectra 900) obtained from Allied Signal were used in this study. The drawing experiments were conducted with an originally designed apparatus shown in Figure 1. The apparatus was mounted on a universal tensile testing machine (Instron model 1333) and was constructed primarily of standard high-pressure fittings. The apparatus was able to make *in situ* force measurements with a calibrated stainless steel cantilever beam and a linear variable-displacement transducer. As depicted in Figure 1, the mechanical grips were located inside a high-pressure vessel and were directly attached to the movable piston of the Instron.

A high-pressure $CO_2$ pump (Hydro-Pac, Inc.) with a maximum discharge pressure of 286.84 MPa was used to introduce ultrahigh-purity $CO_2$ into the system. Specific control over the pressure was maintained during the experiment. The signals and crosshead displacements were monitored with a personal computer with MTS Teststar II software. The initial cross-sectional area was determined both with scanning electron

microscopy (SEM) images of the specimens and by the ratio of the linear density of the fibers to the density of the undrawn UHMWPE fiber (0.97 kg/$m^3$). The strain was calculated from the relative displacement between the crosshead and the beam divided by the original specimen gauge length. All the drawing experiments were conducted at a deformation rate of 0.01 m/60 s, and the sample gauge length was kept at 0.060 ± 0.005 m.

Single-filament tests were performed on an Instron 1123 universal testing machine. The specimens (0.020 ± 0.002 m) were cut and tested at a deformation rate of 10%/60 s. The fiber diameter was estimated either with a high-magnification optical microscope calibrated with a micrometer scale or with the corresponding SEM images of the tested specimen. Because of the negligible adhesion of UHMWPE fibers to commercially available epoxy adhesives, a special mechanical grip was designed for these measurements. In this grip, both ends of the fiber were wrapped around two small stainless steel cylinders (1.27 cm long and 0.32 cm in diameter), which were previously polished to prevent friction. Both cylinders were then placed on the base of the grip and were tightened with two independent screws on each side. The original design of this grip prevented any slippage of the fiber during the deformation.

Differential scanning calorimetry (DSC) experiments were conducted with a TA Instruments 2100 DSC thermal analyzer at a heating rate of 1 °C/min to analyze the thermal behavior of the samples. The overall morphology of these samples was investigated with a JEOL CS-35 scanning electron microscope with a filament voltage of 20,000 V. Wide-angle X-ray scattering (WAXS) experiments were performed with a Statton camera device on a Rigaku RU-200 rotating-anode diffractometer with Fuji As-Va image plates at an operating voltage of 40,000 V and with a total current of 0.030 A under vacuum conditions. The geometry of the measurements was such that the fibers were placed perpendicular to the direction of the beam.

## RESULTS AND DISCUSSION

### *In Situ* Drawing Behavior

A representative drawing behavior for UHMWPE fibers is depicted in Figure 2. A typical elastic region is observed in which all the filaments in the bundle deform uniformly. The upper limit of this region is depicted by a strain ($\epsilon_1$) and a stress ($\sigma_1$) that describe the conditions under which the first filament of the bundle fails. Beyond this point, the subsequent failure of a few additional filaments in the bundle is observed at various stress levels, up to a certain value $\sigma_f$, defined as the draw stress. $\sigma_f$ represents the stress at which the remaining filaments in the bundle are homogeneously deformed up to a maximum strain ($\epsilon_f$) before a catastrophic failure of the sample. $\epsilon_f$ is used to estimate the maximum draw ratio obtained in the sample.

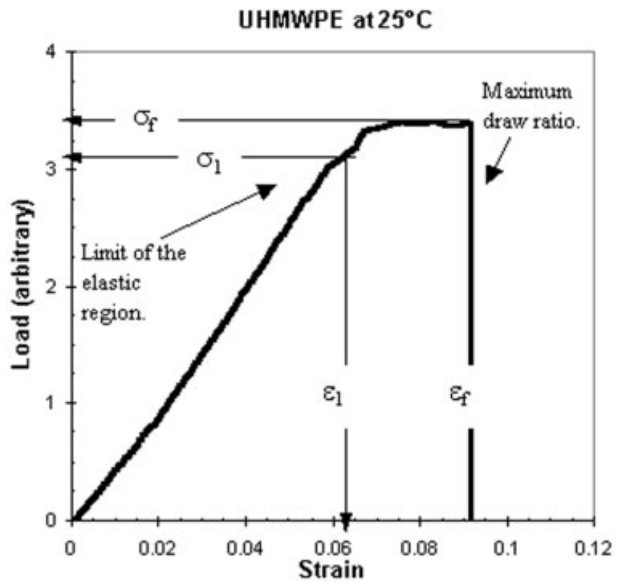


**Figure 2.** Typical drawing behavior of a UHMWPE fiber bundle.

The drawing behavior of UHMWPE fibers treated in $scCO_2$ (20.68 MPa) is compared to that observed at ambient pressures within a certain temperature range. The results indicate that the drawing behavior is completely modified by the presence of $scCO_2$. From Figure 3, it is evident that the drawing behavior in air is highly temperature-dependent. An increase in the drawing temperature substantially reduces both the apparent modulus and $\sigma_f$. The value of $\sigma_f$ decreases from 308 MPa at 25 °C to 224 MPa at 80 °C. It is convenient to point out that in this case a maximum processing temperature of 80 °C is observed. This limiting temperature corresponds to the $\alpha$ transition of polyethylene, which for these fibers is located in a rather small temperature range (80–83 °C) because of their high orientation and

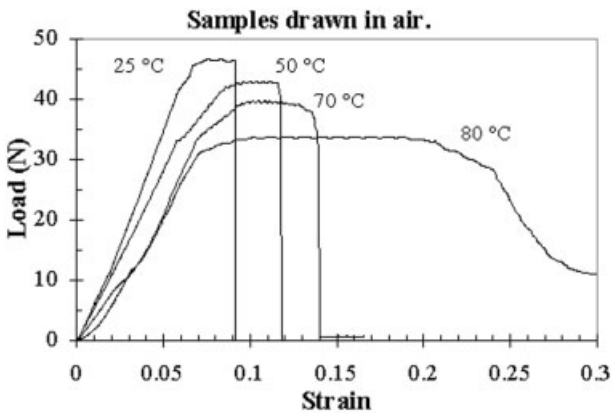


**Figure 3.** Drawing behavior of UHMWPE fibers deformed in air at different temperatures.

crystallinity.[18] The $\alpha$ transition is generally related to movements of the polymer chains within the crystals; this substantially reduces the mechanical integrity of a fiber.

This behavior differs from that observed in the presence of $scCO_2$. As depicted in Figure 4, neither the apparent modulus nor $\sigma_f$ is affected by an increase in the drawing temperature. Clearly, the temperature dependence previously observed for the air-drawn samples is completely suppressed by the deformation being conducted in $scCO_2$. In contrast to what it is observed for the air-drawn samples, the value of $\sigma_f$ remains constant at 286 MPa over the entire range. In addition, the processing range of these fibers is increased up to a temperature of 110 °C; that is, a 30 °C increase in the processing range is obtained when the deformation is performed in $scCO_2$.

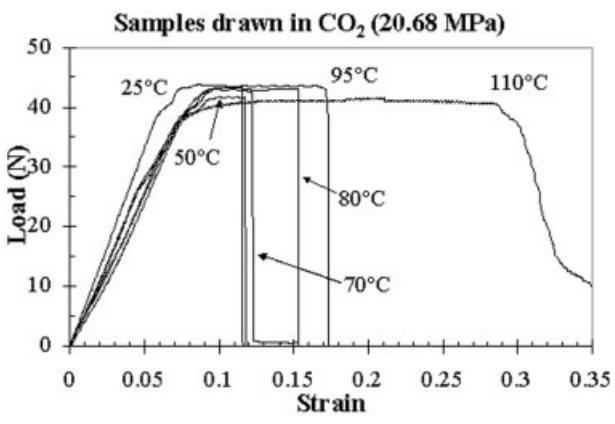


**Figure 4.** Drawing behavior of UHMWPE fibers deformed in the presence of $CO_2$ at different temperatures.

**Table 1.** Maximum Draw Ratios of UHMWPE Fibers Deformed at Different Processing Conditions

| | Draw Ratio | |
|---|---|---|
| Drawing Temperature (°C) | Air-Drawn Samples | $scCO_2$-Drawn Samples |
| 25 | 1.06 | 1.08 |
| 50 | 1.08 | 1.08 |
| 70 | 1.16 | 1.12 |
| 80 | 1.24 | 1.13 |
| 95 | — | 1.16 |
| 110 | — | 1.35 |

The maximum draw ratios estimated from $\epsilon_f$ are summarized in Table 1. These results show that the maximum draw ratio increases in a significant way with temperature. In general, for a given temperature, higher deformations are obtained without $scCO_2$. These results suggest that the mechanical properties of these fibers are maintained when the sample is processed in $scCO_2$.

The initial elastic region is quantitatively described in Table 2 and Figure 5. A constant value of $\sigma_1$ (ca. 255 MPa) is observed along the entire range for processing in $scCO_2$, as shown in Table 2. In contrast, for the air-drawn samples, a clear temperature dependence is observed, $\sigma_1$ being reduced from 280 to 206 MPa when the drawing temperature is increased to 80 °C. However, Figure 5 shows that the limiting strain of the elastic region ($\epsilon_1$) seems to be independent of the presence of $scCO_2$, suggesting that the drawing temperature is the predominant factor for the value of $\epsilon_1$.

**Table 2.** $\sigma_1$ Values for UHMWPE Fibers Drawn at Different Conditions

| Sample | Drawing Temperature (°C) | $\sigma_1$ (MPa) |
|---|---|---|
| Air-drawn | 25 | 280 |
| Air-drawn | 50 | 219 |
| Air-drawn | 70 | 222 |
| Air-drawn | 80 | 206 |
| $CO_2$-drawn | 25 | 259 |
| $CO_2$-drawn | 50 | 251 |
| $CO_2$-drawn | 70 | 263 |
| $CO_2$-drawn | 80 | 252 |
| $CO_2$-drawn | 95 | 256 |
| $CO_2$-drawn | 110 | 255 |

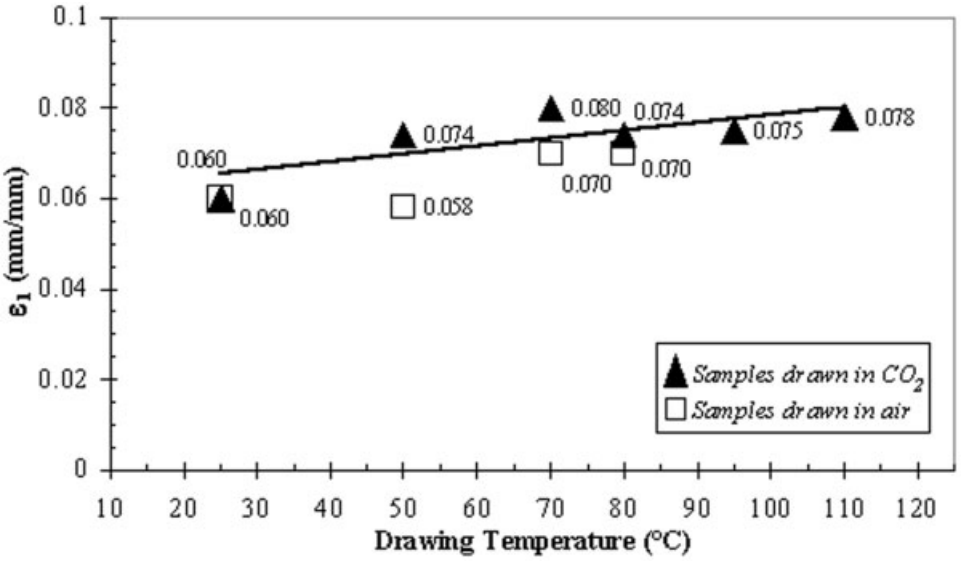


**Figure 5.** $\epsilon_1$ of UHMWPE fibers deformed at different processing conditions.

## DSC

DSC experiments have been conducted over a temperature range of 25–210 °C at a slow heating rate (1 °C/min) to increase the precision of the detection of the thermal transitions of the UHMWPE samples. As depicted in Figures 6 and 7, two melting endotherms are detected in all samples. At approximately 142 °C, a large endotherm corresponding to the characteristic transition involving the melting of crystals in an orthorhombic unit cell is observed. In addition, another endotherm is observed at 150 °C, corresponding to the transition of crystals in a hexagonal unit cell to the melt phase. The presence of this hexagonal phase, as described in the literature,[19,20,23] is mainly associated with the presence of a highly oriented structure and is typically observed in samples processed under high pressure.

As depicted in Figure 6, a considerable growth of the melting endotherm at 150 °C with increasing temperature is observed in the air-drawn samples. This result suggests an apparent development of the hexagonal phase for these samples with the drawing temperature increasing. In contrast, Figure 7 shows that samples treated in $scCO_2$ maintain their crystalline composition, showing no difference in their thermal behavior over the entire range of processing temperatures.

The total crystallinity of the samples is estimated by the ratio of the melting enthalpy of both

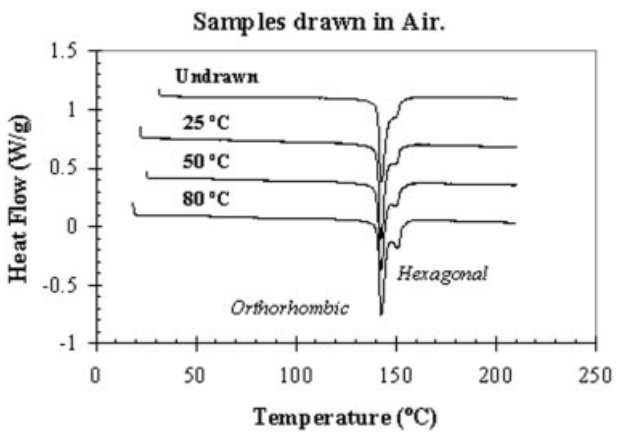


**Figure 6.** Thermal behavior of samples drawn in air at different temperatures.

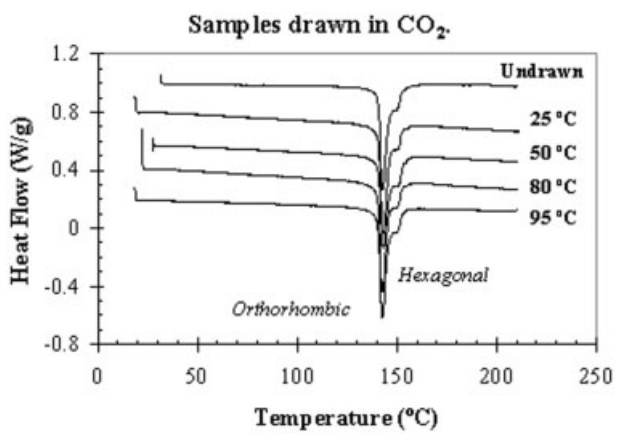


**Figure 7.** Thermal behavior of samples drawn in $scCO_2$ at different temperatures.

**Table 3.** Crystallinity Changes for UHMWPE Fibers Drawn at Different Conditions

| Sample | Drawing Temperature (°C) | Crystallinity (%) |
|---|---|---|
| Undrawn UHMWPE | — | 90.1 |
| Air-drawn | 25 | 91.2 |
| Air-drawn | 50 | 95.2 |
| Air-drawn | 70 | 96.1 |
| Air-drawn | 80 | 98.7 |
| $CO_2$-drawn | 25 | 91.0 |
| $CO_2$-drawn | 50 | 92.6 |
| $CO_2$-drawn | 80 | 93.7 |
| $CO_2$-drawn | 95 | 93.3 |

endotherms and the heat of fusion for polyethylene ($288.89 \times 10^3$ J/Kg). As presented in Table 3, the crystallinity of air-drawn samples increases considerably up to a value of 98% at higher drawing temperatures. In contrast, no significant changes are observed in the crystallinity of $scCO_2$-treated samples. These results suggest that $scCO_2$ helps to maintain the integrity of the crystalline phase, even though it does not interact with it.

No changes in the apparent melting points are observed, regardless of the processing conditions; this suggests that the imposed deformation does not promote changes or alterations to the crystalline phase. In all cases, a second DSC scan shows a broad melting peak around 139 °C, showing that the high orientation of the sample is destroyed during the melting process.

## SEM

SEM analysis has been employed to analyze the macroscopic morphology of the deformed materials. SEM images have been used to estimate and compare the amount of macroscopic damage created by the deformation and its relation to the processing conditions. As shown in Figure 8, the general morphology of these fibers is characterized by a considerably smooth surface, with no evident flaws even at higher magnifications. These factors arise as a result of the highly oriented structure of the fibers. Fibers $20–30 \times 10^{-6}$ m in diameter with no significant polydispersity size characterize this material. Also from this figure, it is evident that, regardless of the processing conditions, no significant changes in the general morphology can be observed. The imposed deformation and, in some cases, the hydrostatic pressure have no significant effect on the smoothness and orientation of the material. These observations suggest that the differences between materials processed at different conditions become apparent at a smaller length scale, without promoting significant changes in the macroscopic morphology of the fiber.

## WAXS

WAXS experiments have been employed both to quantify the crystalline composition of the samples and to estimate the effects of the deformation on the crystal integrity of the samples. The geometry of the measurements is such that the fibers are placed perpendicular to the direction of the beam.

The scattering pattern of the undrawn fiber is compared to that of fibers drawn at different conditions. The results are presented in Figure 9. Well-defined reflections are obtained for all samples, evidence of their highly oriented structure. The high orientation remains unchanged, regardless of the processing conditions. The strong reflections dominate completely the scattering pattern with almost no sign of an amorphous halo, corroborating the high values of crystallinity, as suggested by DSC.

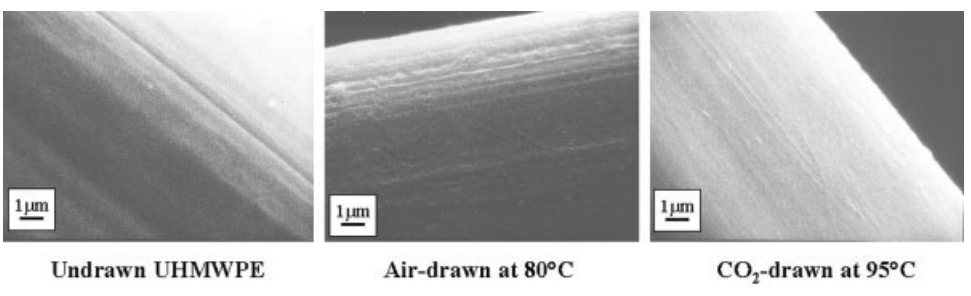


**Figure 8.** SEM images of UHMWPE fibers processed at different conditions.

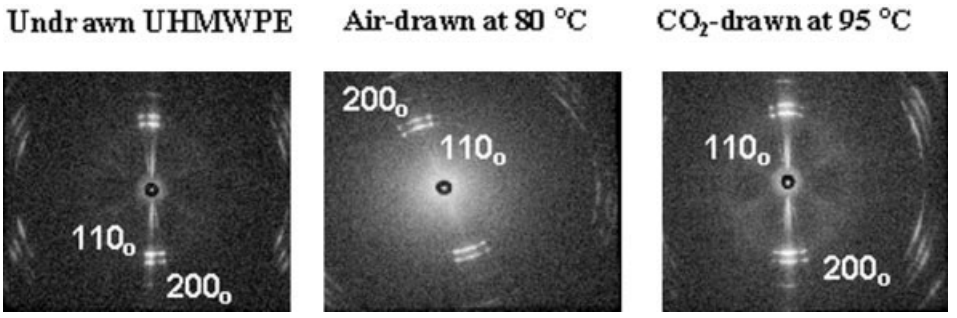


**Figure 9.** WAXS analysis of UHMWPE fibers drawn at different conditions.

Two principal reflections are observed in all cases. As shown in Table 4, the *d*-spacings of these reflections match an orthorhombic type of unit cell (4.10 and 3.70 Å, respectively). The first reflection corresponds to the $110_o$ plane in an orthorhombic unit cell, a reflection typically observed in polyethylene.[20,23] The second reflection is assigned to the $200_o$ plane, also from an orthorhombic unit cell. In contrast of what is observed in the DSC experiments, the presence of the hexagonal phase in the air-drawn samples deformed at higher temperatures is not confirmed by WAXS. No reflections are assigned to a hexagonal type of unit cell, and this shows that the hexagonal phase is not present in any of these samples at ambient conditions.

## Mechanical Properties

The final properties of fibers drawn at different conditions have been determined by single-fiber mechanical tests. The elastic modulus, strain at break, and break stress or tensile strength have been calculated from the responses of at least 10 identical specimens tested under the same conditions. The results are summarized in Table 5 and Figure 10.

**Table 4.** Typical *d*-Spacings in Polyethylene and Their Comparison with the Observed Reflections

| Sample | *d*-Spacing (Å) | *d*-Spacing (Å) |
|---|---|---|
| Theoretical orthorhombic | 4.10 ($110_o$) | 3.70 ($200_o$) |
| Theoretical monoclinic | 4.55 ($100_o$) | — |
| Theoretical hexagonal | 4.33 ($100_o$) | — |
| Undrawn UHMWPE | 4.101 | 3.703 |
| Air-drawn at 80 °C | 4.136 | 3.740 |
| $CO_2$-drawn at 95 °C | 4.128 | 3.720 |

Evidently, the mechanical response of samples treated in $scCO_2$ remains approximately constant with increasing temperature. Both the elastic modulus and the strain at break remain unchanged at 50 GPa and 3.5%, respectively, over the entire temperature range. This suggests again that the high-pressure environment created by the presence of $scCO_2$ helps to maintain the mechanical integrity of the fiber; therefore, the macroscopic deformation required to break the sample remains unaltered, regardless of the processing conditions.

In contrast, the behavior for the air-drawn samples is completely different. The mechanical properties are very temperature-dependent in this case. Both the elastic modulus and tensile strength are reduced in a significant manner with increasing temperature. Almost a 45% decrease in the elastic modulus along with a 13% reduction in the tensile strength is observed with the processing temperature increasing to 80 °C. The larger draw ratios observed in these samples correlate with their higher crystallinity, as described later.

As depicted in Figure 10, it seems that the macroscopic deformation imposed by drawing promotes an overall decrease in the mechanical properties with respect to the undrawn sample. For the specific case of the $scCO_2$-drawn samples, this reduction in the mechanical properties is compensated by the fact that the processing range is increased to a considerable degree (30 °C).

These results overall suggest that the deformation in $scCO_2$ is different from that observed at ambient pressure. The high pressure, along with the presence of $scCO_2$, promotes significant differences in the deformation process, which are reflected in the final thermal and drawing behavior. Drawing in air appears to involve the deformation of an orthorhombic unit cell along the entire pro-

**Table 5.** Single-Filament Properties of UHMWPE Fibers at Different Processing Conditions

| Sample | Modulus (GPa) | Strain at Break (%) | Break Stress (MPa) |
|---|---|---|---|
| Undrawn UHMWPE | 69.9 | 2.7 | 1672 |
| 25 °C in air | 55.4 | 3.15 | 1528 |
| 50 °C in air | 52.2 | 3.26 | 1503 |
| 70 °C in air | 45.1 | 4.14 | 1409 |
| 80 °C in air | 30.8 | 4.70 | 1334 |
| 25 °C in $CO_2$ | 52.4 | 3.40 | 1522 |
| 50 °C in $CO_2$ | 51.1 | 3.39 | 1512 |
| 70 °C in $CO_2$ | 50.2 | 3.42 | 1509 |
| 80 °C in $CO_2$ | 50.1 | 3.46 | 1485 |
| 95 °C in $CO_2$ | 48.9 | 3.57 | 1452 |
| 110 °C in $CO_2$ | 46.9 | 3.55 | 1421 |

cess. The macroscopic deformation imposed on the sample promotes some strain-induced crystallization, which is responsible for the increased crystallinity of these samples, as detected by DSC. The deformation is highly temperature-dependent in this case, as judged by the considerable increase in the draw ratios for air-drawn samples. In this case, the addition of new crystals to the existing crystalline lamellae is restricted because of the low mobility of chains within the orthorhombic unit cell. The newly formed crystals grow either between the existent lamellae or as extended single chains, this later possibility being specifically valid for polyethylene.[23] These two situations inevitably promote internal constraints in the sample. In any of these cases, the newly formed orthorhombic crystals will tend to expand to the more mobile hexagonal phase during heating before transforming into the melt phase, relaxing the stress imposed by the constraints.[20] This is the reason for the appearance of the melting endotherm at 150 °C in these samples during the DSC experiments. At ambient conditions, however, no hexagonal phase is present and only the orthorhombic unit cell is present, as confirmed by WAXS.

The deformation in $scCO_2$ appears to involve a crystal–crystal transformation, from the orthorhombic unit cell to the more mobile hexagonal phase, because of the high-pressure environment (20.7 MPa). It is well known that the mobility of the hexagonal phase is related to the degrees of freedom for rotations around the *c* axis of the fiber but that the deformation along the chain backbone is somewhat restricted.[19,20] If, as suggested, a hexagonal phase is formed in this case, lower macroscopic uniaxial deformations would be expected for $scCO_2$-treated samples. This is actually in agreement with the lower draw ratios observed experimentally. As a result, the amount of strain-induced crystallization would also be reduced, and this suggests that the crystallinity of these samples must remain unchanged with increasing drawing temperature, something also confirmed by DSC. Furthermore, because the hexagonal phase melts at a higher temperature,[19] the presence of this phase with drawing in $scCO_2$ explains the observed increase in the processing temperature range. This suggests that either the presence of $scCO_2$ or the imposed hydrostatic pressure suppresses the $\alpha$ transition of UHMWPE fibers, shifting it to higher temperatures through a crystal–crystal transformation to the hexagonal phase.

In contrast to the air-drawn samples, the newly formed crystals are added to the existing crystalline lamellae without internal constraints because of the high mobility of the hexagonal phase. Therefore, no change in the thermal behavior is expected for samples treated in $scCO_2$ at different temperatures, as also confirmed experimentally by DSC. During depressurization, crystals within the sample return to the original orthorhombic phase, as suggested by WAXS.

## CONCLUSIONS

The drawing behavior of UHMWPE fibers in $scCO_2$ has been compared to that in air at different temperatures. Both the mechanical properties

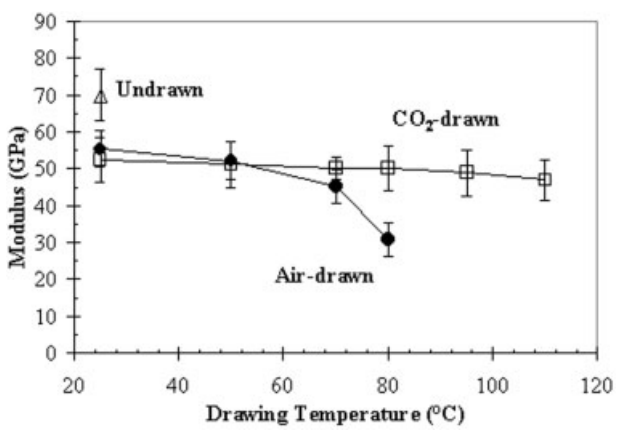


**Figure 10.** Elastic modulus of UHMWPE fibers treated at different processing conditions.

and drawing behavior are altered when the deformation is conducted in the presence of $scCO_2$. Samples drawn in air show significant temperature dependence in their drawing properties. In contrast, $scCO_2$-drawn samples show a constant value of $\sigma_f$ (286 MPa) and the tensile strength (1500 MPa) over the entire temperature range. Apparently, the $scCO_2$ environment, along with the imposed hydrostatic pressure, helps to maintain the integrity of the fibers, allowing them to deform up to a certain extent without changes in $\sigma_f$. The modulus, strain at break, and tensile strength are essentially unaltered when the fiber is drawn in $scCO_2$, whereas significant weakening is observed for air-drawn samples with increasing temperature.

The thermal behavior of air-drawn samples is also dependent on the drawing temperature. DSC results show the development of a melting endotherm at 150 °C for air-drawn samples when increasing drawing temperature, suggesting the possibility of the development of an apparent hexagonal phase. In addition, a significant increase in crystallinity is observed in these samples. In contrast, no significant changes in the thermal behavior are observed in the $scCO_2$-treated samples. Apparently, the presence of $scCO_2$ promotes the integrity of the crystalline phase remaining unaltered, regardless of the processing conditions.

WAXS results, however, suggest that no hexagonal phase is present at ambient conditions in any of the samples, regardless of the processing conditions. An orthorhombic unit cell is present in all the samples, showing two strong reflections ($110_0$ and $200_0$), with no trace of the suggested hexagonal phase.

These results suggest that the appearance of the high-temperature melting peak in DSC is related to the internally constrained manner in which air-drawn samples crystallize. In contrast, samples deformed in $scCO_2$ are able to crystallize without internal constraints via the mobile hexagonal phase. The existence of this hexagonal unit cell during deformation in $scCO_2$ is consistent with the lower draw ratios experimentally confirmed for these samples, as well as the processing temperature increased up to 110 °C.

The authors acknowledge the U.S. Army Soldier Systems Command RD&E Center for providing the materials for this study. Support for this study was also provided by the Materials Research Science and Engineering Center at the University of Massachusetts.

## REFERENCES AND NOTES

1. Porter, R. S.; Wang, L. J Macromol Sci Rev Macromol Chem Phys 1995, 35, 82.
2. Kavesh, S.; Prevorsek, D. C. Int J Polym Mater 1995, 30, 15–56.
3. Nakae, M.; Uehara, H.; Kanamoto, T.; Ohara, T.; Porter, R. S. J Polym Sci Part B: Polym Phys 1999, 37, 1921–1930.
4. Lee, D.; Chen, W.; Yeh, M.; Chen, T. Polym Eng Sci 1995, 35, 19, 1546–1554.
5. Brennecke, J. F. Nature 1997, 389, 333–334.
6. Blanchard, L. A.; Hancu, D.; Beckman, E. J.; Brennecke, J. F. Nature 1999, 399, 28–29.
7. Sarbu, T.; Styranec, T.; Beckman, E. J. Nature 2000, 405, 165–168.
8. Leitner, W. Nature 2000, 405, 129–130.
9. Adam, D. Nature 2000, 407, 938–940.
10. Shieh, Y.; Su, J.; Manivannan, G.; Lee, P. H. C.; Sawan, S. P.; Spall, W. D. J Appl Polym Sci 1996, 59, 695–705.
11. Shieh, Y.; Su, J.; Manivannan, G.; Lee, P. H. C.; Sawan, S. P.; Spall, W. D. J Appl Polym Sci 1996, 59, 707–717.
12. Cooper, A. I.; Londono, J. D.; Wignall, G.; McClain, J. B.; Samulski, E. T.; Lin, J. S.; Dobrynin, A.; Rubinstein, M.; Burke, A. L. C.; Fréchet, J. M.; DeSimone, J. M. Nature 1997, 389, 368–371.
13. Zachariades, A. E.; Porter, R. S. J Appl Polym Sci 1979, 24, 1371.
14. Beckman, E. J.; Porter, R. S. J Polym Sci Part B: Polym Phys 1987, 25, 1511–1517.
15. Hobbs, T.; Lesser, A. J. J Polym Sci Part B: Polym Phys 1999, 37, 1881–1891.
16. Hobbs, T.; Lesser, A. J. Polymer 2000, 41, 6223–6230.
17. Hobbs, T.; Lesser, A. J. Polym Eng Sci 2001, 41, 2, 135–144.
18. Takayanagi, M.; Imada, K.; Nagai, A.; Tatsumi, T.; Matsuo, T. J Polym Sci Part C: Polym Symp 1967, 16, 867–876.
19. Rastogi, S.; Kurelec, L.; Lemstra, P. J. Macromolecules 1998, 31, 5022–5031.
20. Kurelec, L.; Rastogi, S.; Meier, R. J.; Lemstra, P. J. Macromolecules 2000, 33, 5593–5601.
21. Tashiro, K.; Sasaki, S.; Kobayashi, M. Macromolecules 1996, 29, 7460–7469.
22. Kuwabara, K.; Horii, F. Macromolecules 1999, 32, 5600–5605.
23. Peacock, A. J. Handbook of Polyethylene: Structures, Properties and Applications; Marcel Dekker: New York, 2000.